



Promote the conductivity of solid polymer electrolyte at room temperature by constructing a dual range ionic conduction path

Ruiyang Li^a, Haiming Hua^a, Yuejing Zeng^a, Jin Yang^a, Zhiqiang Chen^b, Peng Zhang^{b,*}, Jinbao Zhao^{a,b,*}

^a College of Chemistry and Chemical Engineering, State–Province Joint Engineering Laboratory of Power Source Technology for New Energy Vehicle, State Key Laboratory of Physical Chemistry of Solid Surfaces, Engineering Research Center of Electrochemical Technology, Ministry of Education, Collaborative Innovation Center of Chemistry for Energy Materials, Xiamen University, Xiamen 361005, Fujian, China

^b College of Energy, Xiamen University, Xiamen 361102, Fujian, China

ARTICLE INFO

Article history:

Received 22 January 2021

Revised 13 April 2021

Accepted 23 April 2021

Available online 4 May 2021

Keywords:

Solid polymer electrolyte

Amorphous polymer

Ionic conductivity

Room temperature

Arrhenius equation

ABSTRACT

Poly(ethylene oxide) (PEO) is a classic matrix model for solid polymer electrolyte which can not only dissociate lithium-ions (Li^+), but also can conduct Li^+ through segmental motion in long-range. However, the crystal aggregation state of PEO restricts the conduction of Li^+ especially at room temperature. In this work, an amorphous polymer electrolyte with ethylene oxide (EO) and propylene oxide (PO) block structure (B-PEG@DMC) synthesized by the transesterification is firstly obtained, showing an ionic conductivity value of 1.1×10^{-5} S/cm at room temperature (25 °C). According to the molecular dynamics (MD) simulation, the PO segments would lead to an inconsecutive and hampered conduction of Li^+ , which is not beneficial to the short range conduction of Li^+ . Thus the effect of transformation of aggregation state on the improvement of ionic conductivity is not enough, it is necessary to further consider the different coupled behaviours of EO and PO segments with Li^+ . In this way, we blend this amorphous polymer (B-PEG@DMC) with PEO to obtain a dual range ionic conductive solid polymer electrolyte (D-SPE) with further improved ionic conductivity promoted by constructing a dual range fast ionic conduction, which eventually shows a further improved ionic conductivity value of 2.3×10^{-5} S/cm at room temperature.

© 2021 Science Press and Dalian Institute of Chemical Physics, Chinese Academy of Sciences. Published by ELSEVIER B.V. and Science Press. All rights reserved.

Introduction

In the past two decades, lithium ion batteries have been widely used in people's daily lives, including portable electronic products, electric vehicles and grid energy storage systems [1]. Moreover, as countries accelerate the process of replacing traditional fossil energy with renewable energy, the demand for large scale energy storage system with high energy density has greatly increased [2]. The improvement of battery energy density also puts forward higher requirements for battery safety [3]. Currently, the electrolyte used in traditional liquid batteries is ester electrolyte, which has safety problems such as low vapor pressure, flammability, and easy leakage. This potential safety hazard hinders the development of high specific energy batteries [4–7].

As a result, solid electrolytes (including ceramic electrolytes and polymer electrolytes) are considered to be one of the effective ways to improve safety issues [8–11]. Compared with ceramic

electrolytes, the solid polymer electrolytes (SPEs) can be adapted to the current traditional battery assembly process due to its better processability. As expected, the Bolloré company firstly prepared the commercial solid power battery assembled with poly(ethylene oxide) (PEO) polymer electrolyte for use on the “Bluecar” [12].

Up till now, PEO has been the most widely used polymer electrolyte matrix material for SPEs since it was firstly reported by Wright in 1973 [13]. The main reason for making PEO irreplaceable for decades should attribute to ethylene oxide (EO) segments of PEO. On one hand, the ether oxygen atoms in the EO chain can interact with the cations such as Li^+ which makes PEO have an extremely strong dissociating property for a wide variety of salts. On the other hand, the excellent chain flexibility and segmental motion ability of EO segments ensure the conduction of Li^+ . Unfortunately, the aggregation state of PEO at room temperature is semi-crystalline which greatly limits the conduction of Li^+ in PEO. The ionic conductivity curve of PEO always shows a classic polyline with three segments with the temperature increasing. The first segment appears at the temperature which is far below 65 °C (melting point of PEO), and the ionic conductivity is extremely low (10^{-8} – 10^{-7} S/cm) because of the crystallization. During

* Corresponding authors.

E-mail addresses: pengzhang@xmu.edu.cn (P. Zhang), jzbhao@xmu.edu.cn (J. Zhao).

the second segment, the ionic conductivity rapidly increases when the temperature ranges from 50 to 70 °C in which the aggregation state of PEO is changing from crystalline to amorphous. Once the temperature is far above 65 °C, the third segment shows a flat line. Above all, due to the fact that the aggregation state of PEO changes with the temperature, the ionic conductivity curve of PEO shows a classic polyline with three segments. Particularly, the existence of non-conducting crystalline phase at room temperature greatly limits the segmental motion and the conduction of Li⁺ [14–16]. Therefore, improving the room temperature conductivity of polymer electrolytes is the focus of polymer electrolyte research.

A variety of strategies have been brought out to improve the ionic conduction performance of PEO-based SPE such as introduction of fillers [17–21], block copolymers [22], and cross-linking networks [23,24]. Nevertheless, most of strategies only considered the aggregation state of PEO, but ignored the interaction between the ionic mobility and dynamics of chains. It is necessary to find a way to improve the aggregation structure of PEO from crystallization to amorphous, and build a continuous conduct pathway of Li⁺ at the same time.

Naturally, poly(propylene oxide) (PPO) based polymers which have a similar molecular structure to PEO is worth considering. PPO with the randomly distributed methyl groups can easily lead to an amorphous macromolecular structure which is beneficial to the short-range conduction of Li⁺. In this way, plenty of studies have been done [25–27]. Especially, in 2018, Vidal's group [25] found that the oligomer PEO-PPO-PEO based triblock polymer electrolyte shows a highly fitting to Arrhenius model which is beneficial to the improvement of room temperature ionic conductivity of PEO based SPE.

On the other hands, considering the formation of uniform and continuous Li⁺ transport channels on the molecular-scale, the modified solid-state organic fillers should be chosen. Recently, alternative polymer electrolyte has been focused on such as polycarbonates, polynitriles, polyalcohols or polyamines [28]. In particular, polycarbonates show excellent stability and electrochemical performance [29,30]. This makes it feasible for operation of solid polymer electrolyte in lithium batteries at room temperature. In 2017, Cui et al. [31] linked carbonyl group with 2–3 ethylene oxide which shows ionic conductivities in the range of 10⁻⁵ S/cm at room temperature with addition of cellulose.

Furthermore, in 2018, Mecerreyes et al. [32] synthesised a series of poly(ethylene oxide)/carbonate polymers with different amount of EO units, and the optimal composition (34 units of EO) is found which shows an ionic conductivity value around 10⁻⁵ S/cm at 25 °C, however, the presence of crystal region could not decrease the crystallinity with the increase of the amount of EO units. As mentioned above, the incorporation of propylene oxide (PO) units in polymer chains is a very effective way to prevent the crystallization, however, too many PO units would limit

the conduction of Li⁺ owing to the steric hindrance caused by methyl group. Compared to EO segments, PO segments could prevent the crystallization but the methyl group in PO segments would limit the ionic conductive ability of –OCH₂CH₂O–, in brief, PO segments could not conduct Li⁺ smoothly because of limitation of methyl group which could only conduct ions in a short range. Thus a new strategy of promoting ionic conduction needs to be brought out. In order to improve the ionic conductivity of PEO, taking aggregation state into consideration only is not enough. It's also necessary to consider the interaction between the ionic mobility and dynamics of chains by constructing continuous Li⁺ conductive pathway on both short and long range [33–35].

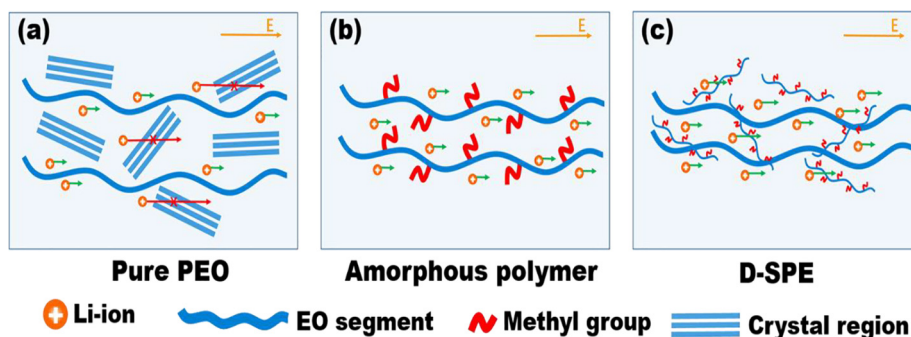
From the above, the ionic conductivity of PEO could be improved in two ways: Firstly, transform the aggregation state of PEO from semi-crystalline to amorphous by introducing the PEO-PO-PEO based triblock polymer chain. Secondly, construct a continuous conduction pathway of Li⁺ by introducing a long range ionic conductive EO segment in the PEO-PO-PEO.

In this work (as shown in the Scheme 1), we synthesize an amorphous copolymer containing PO units to promote lithium ion conduction by changing the aggregation of PEO from semi-crystalline to amorphous state with higher segmental motion ability at room temperature. However, with the limits of PO units the Li⁺ could only conduct in short range. Then a continuous and long-range conductive pathway of Li⁺ is built via compounding the low molecular weight PEO. In this way, a solid polymer electrolyte named dual-range ionic conductive solid polymer electrolyte (D-SPE) with both long- and short- range ionic conductive channel is obtained which could conduct Li⁺ more smoothly and continuously. The aggregation state transformation could be investigated by differential scanning calorimetry (DSC). Eventually, the molecular dynamics simulation is used to analyse the interaction between Li⁺ and EO segment (PO segment).

Experimental

Synthesis of the poly(ethylene oxide carbonates) with block structure (B-PEG@DMC) via melt-polycondensation

The synthesis of functional aliphatic polycarbonates via melt polycondensation is a current synthetic method. Transesterification synthesis is the reaction between a diol and dimethyl carbonate at high temperature and vacuum. The synthesis route is mentioned in Fig. 1(a). In this work, we use dimethyl carbonate (DMC) as diester and three diol polymers, poly(ethylene glycol)-b-block-poly(propylene)-block-poly(ethylene glycol), with different molecular weight and different weight fraction of EO segment, named by their average weight molecular, B-PEG(1100), B-PEG(2000) and B-PEG(2900) as diol. The different B-PEG@DMC were synthesised by a 3-step reaction. Firstly, it is necessary to obtain



Scheme 1. The conduct of Li⁺ in different polymers: (a) pure PEO; (b) amorphous polymer; (c) dual-range ionic conductive solid polymer electrolyte (D-SPE).

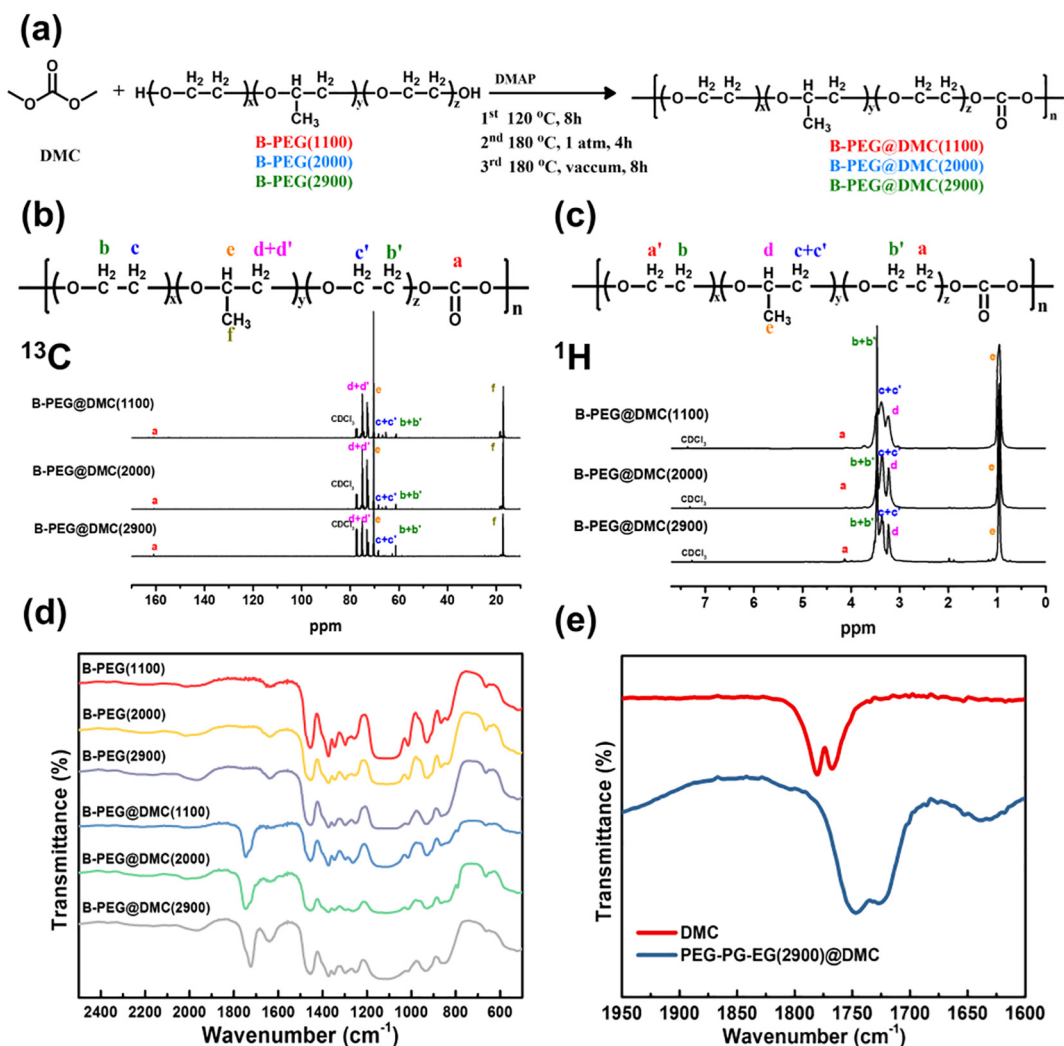


Fig. 1. (a) The synthesis of different poly(ethylene glycol)@ carbonates (B-PEG@DMC). (b) ^{13}C NMR and (c) ^1H NMR spectra of B-PEG@DMC. (d) FTIR of PEG-PG-EG (the monomer) and resulting B-PEG@DMC and (e) the redshift of B-PEG@DMC (2900) compared to free DMC.

a homogeneous intermediate product via 120 °C stirring for 8 h leading to low molar mass oligomers. Then, the temperature was increased to 180 °C under normal pressures for 4 h aiming to obtain a steady increase of the chain growth without the excessive volatility of low mass precursor. Finally, the excess of DMC and the resulting methanol was removed under high vacuum for 8 h at 180 °C. This process is crucial for the high conversions of reaction. After that, all the resultants were dissolved in the dichloromethane, and then precipitated in cold diethyl ether with a yield above 87% in all cases.

Preparation of the amorphous solid polymer electrolyte (B-PEG@DMC) membrane

As shown in the Fig. S1, B-PEG@DMC with different ratios of lithium bis(trifluoromethanesulfonyl) imide (LiTFSI) (Alfa Aesar Co., China) were dissolved together in the anhydrous acetonitrile (ACN, Aladdin). Stirring intensely for 8 h to obtain a 10 wt% (the weight fraction of solid) homogeneous solution. After that the moderate solution was dropped into the nylon porous membrane and drying under vacuum at 80 °C for 12 h. Finally, the dry B-PEG@DMC membrane, B-PEG@DMC(x)-y was prepared, where x and y represent the molecular weight of diol monomers and the O/Li mole ratio.

Preparation of the dual range ionic conductive solid polymer electrolyte (D-SPE) membrane

PEO (number-average molecular weight, $M_n = 100,000$, Aladdin) and B-PEG@DMC with LiTFSI were mixed together in the ACN stirring intensely overnight to obtain a 10 wt% homogeneous slurry in the same method as shown in Fig. S1. After that the slurry was dropped into the nylon porous membrane and drying in vacuum oven at 80 °C for 12 h. The dried D-SPE membrane (PEO-x-y) was prepared, where x and y represent the weight ratio of B-PEG@DMC(2900) and the O/Li mole ratio.

Assemble and measurements of the batteries

In this study, all the cell tests were carried out using CR2016 (CR2032)-type coin cells (CR2016 for lithium-ion batteries and CR2032 for Li symmetric batteries). First, the LiFePO_4 (LFP) cathode is placed in the positive shell, then, the solid polymer electrolyte membrane and the lithium anode were placed in turn. The ionic conductivity testing cells were assembled in the similar way as mentioned above, the only difference is that stainless steel (replacing the LFP cathode and lithium anode) sandwich the D-SPE membrane. All of the batteries were fabricated in a glove box filled with Ar atmosphere. It's worth noting that the LFP cathode is composed of LFP, polyvinylidene fluoride (PVDF), acetylene black (AB) and

succinonitrile (SN) with a weight ratio of 7:1:1:1. The average mass loading of the LFP electrodes were 1.4 mg/cm². Finally, the assembled cells were preheated at 80 °C overnight to form a uniform ionic conductive channel between cathode and electrolyte. A Neware multichannel battery testing system was used to perform electrochemical measurements. Battery cycle performances between 2.5 and 3.8 V at a current rate of 0.2C was measured for 100 cycles at room temperature.

Materials characterization

The differential scanning calorimetry (DSC) curves were conducted on a Model STA 449 instrument (NETZSCH Machinery and Instruments Co., Ltd.) to investigate the enthalpy change of the SPE with a heating rate of 10 K/min. The Fourier transform infrared spectroscopy (FTIR, Thermo Fisher Scientific Inc.) measurement was used to study the molecular information of the diol polymer monomers and B-PEG@DMC in the wavenumber range of 500–3500 cm⁻¹. The weight-average molecular weight (M_w), number-average molecular weight (M_n) and dispersity (D) were determined by gel permeation chromatography (GPC). The cross profile morphology of D-SPE and B-PEG@DMC membranes were observed by a cold-field emission electron microscope (Gemini 500, ZEISS) and the corresponding elemental mapping was obtained by the energy dispersive spectral (EDS) attaching. ¹H and ¹³C nuclear magnetic resonance (NMR) spectra conducted on Bruker 500 MHz at room temperature. The electrochemical stability of SPE was evaluated by the liner scanning voltammetry (LSV) on electrochemical workstation (CHI660E).

The ionic conductivity of B-PEG@DMC and D-SPE was measured by electrochemical impedance spectroscopy (EIS) on an electrochemical Solartron workstation, in the frequency range of 0.1–10⁵ Hz with an amplitude voltage of 10 mV. Finally, the ionic conductivity was calculated from the following formula (1):

$$\sigma = d/(R_b \times A) \quad (1)$$

where σ refers to the ionic conductivity of electrolyte membrane, d refers to the thickness of electrolyte membrane, R_b is the resistance of the electrolyte membrane and A is the area of the stainless steel (SS).

The classical molecular dynamics simulation was performed using GROMACS 2018.8 software [36]. The visualization of structures were performed by VMD software [37]. We employed the OPLS force field [38], which is suitable for electrolyte solution and polymer electrolyte. The force field parameters of each molecule were taken from the literatures [39,40]. Atomic charges of ions were multiplied by scale factor 0.78 to correct the polarization effect of anion and cation [41]. The models of PEO, B-PEG-10 wt% and B-PEG-50 wt% are shown in the Fig. S2. There are 22 polymer chains and 55 LiTFSI in the three electrolyte boxes. These three boxes were generated by Packmol software [42]. All boxes were firstly submitted to energy minimization using the steepest-descent method. The equilibrium simulation was carried out under the NPT ensemble at 1 bar. In order to gain an equilibrium system, an annealing method was used. The system ran at 598.15 K for 20 ns, and then cooled to 353.15 K within 40 ns, then ran at 353.15 K for 20 ns. The production simulation ran for 10 ns at 353.15 K. A time step of 2 fs and a Verlet algorithm were used. An Ewald summation routine was used for long-range forces ($r_{cut} = 10 \text{ \AA}$), and the data were collected every 20 ps. To simulate the ion conductivity, an NPT simulation with an electric field of 0.1 V/nm is performed, and the conductivity is calculated by formula (2), in which v is average drift rate, c is ion concentration, E is electric field strength, Z is ion charge, and F is Faraday constant.

$$\sigma = \frac{|v^+|}{E} \cdot c^+ \cdot |Z^+| \cdot F + \frac{|v^-|}{E} \cdot c^- \cdot |Z^-| \cdot F. \quad (2)$$

Results and discussion

The synthesis route of poly(ethylene carbonates) via transesterification is shown in Fig. 1(a). Fig. 1(b and c) show the ¹³C and ¹H NMR spectra of B-PEG@DMC(1100), B-PEG@DMC(2000), and B-PEG@DMC(2900). ¹³C NMR (CDCl₃): $\delta = 161.0$ (OCOO), 75.2 (OCHCH₃-CH₂), 70.5 (OCHCH₃-CH₂), 68.5 (OCH₂CH₂), 61.3 (OCH₂-CH₂), 17.2 (OCHCH₃-CH₂). ¹H NMR (CDCl₃): $\delta = 4.15$ (OCOOCH₂-CH₂), 3.48–3.25 (m, CH₂O, CHCH₃-CH₂, CHCH₃-CH₂), 0.96 (t, CHCH₃-CH₂). The signal at 161.0 ppm is attributed to the carbon of the carbonate group and that at 61.3 ppm is assigned to the carbon next to the carbonate group. The peaks of methylene groups close to the carbonates could also be observed at 4.15 ppm in ¹H NMR. Up till now, the result of NMR spectrum could preliminarily confirm the formation of the B-PEG@DMC. Unfortunately, the intensity of the methylene groups close to the carbonates (OCOOCH₂CH₂) is influenced by the ratio between EO units and carbonate group, which makes the signal of OCOOCH₂CH₂ at $\delta = 4.15$ ppm in ¹H NMR too weak to be identified in detail (Fig. S3), and thus we will further investigate through FTIR spectrum. These unique molecular structure of B-PEG@DMC makes them similar in the properties of transformation of aggregation state which is beneficial to the conduction of Li⁺ at room temperature, but different in the ionic conductivity. Besides, the molar masses of the B-PEG@DMC were shown in Supplementary data which are characterized by gel exclusion chromatography (GPC). As shown in Table S1, the values of molar masses are ranging from 8342 to 11216. All of them are higher than the monomer, demonstrating that the typical transesterification reaction occurs. As expected, different B-PEG@DMC show almost a similar value of molar masses which could be regarded as an appropriate model to discuss the interaction between the ionic mobility and dynamics of chains of the conduction of Li⁺ in SPE.

In Fig. 1(d and e), the FTIR is used to investigate molecular structure and interactions between groups. Compare B-PEG with B-PEG@DMC (shown in Fig. 1d), the high intensity peak only appears at 1775 cm⁻¹ in the FTIR of B-PEG@DMC which belongs to the characteristic stretching vibration of carbonyl group on DMC. Furthermore, the infrared absorption peak of carbonyl group would be affected by different chemical band around before and after transesterification reaction. The enlarged FTIR views of carbonyl group of B-PEG@DMC(2900) and DMC were shown in Fig. 1(e) as one example to verify that the carbonyl group of B-PEG@DMC is attached to the EG segment. Obviously, the absorption peak of carbonyl group shifts from 1775 cm⁻¹ (belongs to C = O in DMC) to 1740 cm⁻¹ (belongs to the C = O in B-PEG@DMC(2900)). A significant red shift is observed caused by the electron giving effect, attributing to ethylene oxide-block-propylene oxide-block-ethylene oxide (EO-PO-EO) segment in the B-PEG@DMC(2900). This could be a strong evidence for the presence of carbonyl groups attaching to the EO-PO-EO segment. Besides, as an example, the FTIR of B-PEG@DMC(2900) and B-PEG(2900) is shown in Fig. S4, the peaks at 1370 and 1460 cm⁻¹ respectively refer to bending vibration of methyl group and methyne group. The peaks range from 1100 to 1200 cm⁻¹ are assigned to the -C-O-C- stretching vibration. Above all, the results of NMR and FTIR spectra could eventually confirm the formation of B-PEG@DMC and the molecular structure is advantageous to transformation of aggregation state.

The DSC and thermogravimetric analysis (TGA), shown in Fig. 2 (a and b) respectively, were used to determine the thermal properties of B-PEG@DMC(2900). As expected, no melting endo thermic peak is observed ranging from 35 to 100 °C, which indicates there is no crystalline region in B-PEG@DMC(2900). Meanwhile, the TGA curve of B-PEG@DMC(2900) only shows a smooth single-step in

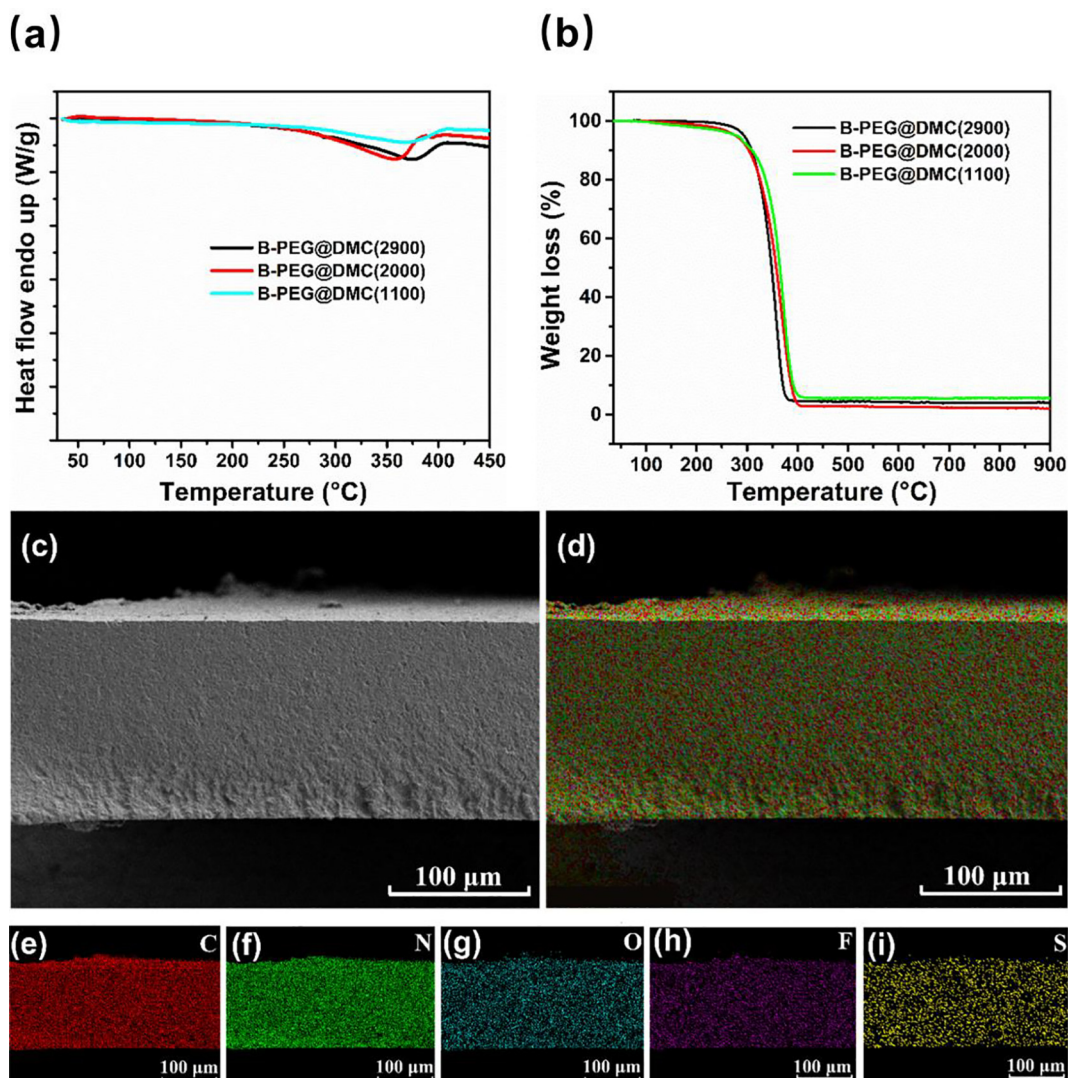


Fig. 2. (a) DSC traces and (b) TGA of the B-PEG@DMC. (c) Cross section SEM images of the B-PEG@DMC membrane. (d) Cross section element distribution and mappings of C, N, O, F, S atoms of the B-PEG@DMC membrane and the corresponding elemental mappings of C (e), N (f), O (g), F (h) and S (i).

the range of 300–400 °C indicating that the B-PEG@DMC(2900) is single component without any residual solvent, which is also consistent with the result of DSC. Therefore, the conduction of Li^+ in the B-PEG@DMC could only attributes to the pure segmental motion of polymer, surely the coupled behaviour of B-PEG@DMC with Li^+ would not be affected by solvent. In addition, the introduce of carbonate group could also be beneficial to the electrochemical stability of SPE (shown in Fig. S11).

In order to obtain a homogeneous membrane for ionic conductivity measurement (Fig. S1), the B-PEG@DMC was mixed with lithium bis(trifluoromethane)sulfonamide (LiTFSI) in ACN solvent, stirred intensely, then casted into the Nylon6 porous membrane. Finally, after vacuum drying the homogenous B-PEG@DMC membrane was obtained. The SEM image (Fig. 2) shows the cross section morphology of B-PEG@DMC membrane. In Fig. 2(c and d), compared with the pristine Nylon6 porous membrane (Fig. S5), the porous membrane is uniformly and completely filled with B-PEG@DMC(2900) and LiTFSI. The stress–strain curves of D-SPE and Nylon porous membrane are shown in Fig. S13 to evaluate the mechanical property of D-SPE. The cross sectional morphology of SEM could confirm that the B-PEG@DMC membrane is obtained

with continuous B-PEG@DMC(2900), which makes the conduction of Li^+ possible. Furthermore, the elemental mapping shows that the C, N, O, F, S elements are evenly distributed in the B-PEG@DMC membrane (Fig. 2e–i). Among them, the N element is unique to nylon membrane and LiTFSI, then C, O elements are common to both nylon membrane and B-PEG@DMC membrane. In particular, the F, S elements, provided by the TFSI^- anion in LiTFSI which is blended in the B-PEG@DMC(2900), also distribute in the membrane, indicating that the B-PEG@DMC(2900) and LiTFSI salts are evenly distributed. Consequently, the cross section morphology of B-PEG@DMC membrane can demonstrate that a continuous Li^+ pathway is successfully built which is satisfied for the further study condition of Li^+ conduction.

In this case, the PO segment of B-PEG@DMC could not only conduct lithium ion but also unblock the restriction of crystal region which is a good way to improve the ionic conductivity at room temperature by transforming the aggregation state of polymer electrolyte. Therefore, the ionic conductivity of B-PEG@DMC was tested as displayed in Fig. 3(a). The ionic conductivity of B-PEG@DMC membrane named as B-PEG@DMC(2900)-15 (with O/Li mole ratio of 15 after optimization shown in Fig. S6 and the x

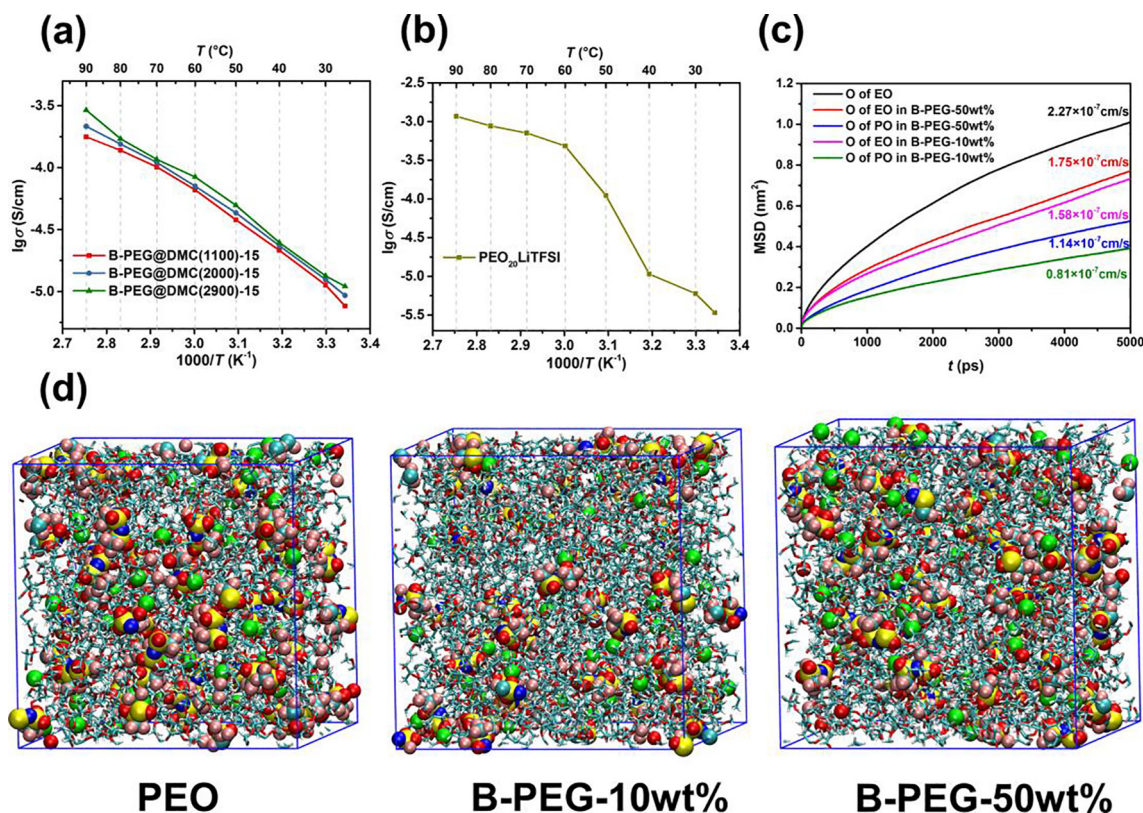


Fig. 3. (a) Arrhenius plots of different B-PEG@DMC(2900)-15 and (b) PEO₂₀LiTFSI. (c) The MSD curve of O atom in different segments. The number next to the curve represents the diffusion coefficient obtained by molecular dynamic simulation. (d) The simulation boxes of lithium salt in PEO and B-PEG. Anions and cations are displayed by balls, and polymer chains are displayed by lines (green: Li atom; yellow: S atom; red: O atom; blue: N atom; pink: F atom; cyan: C atom).

refers to the different molecular weights of diol reactants) are improved at room temperature. It is particularly noteworthy that all the ionic conductivity curves of B-PEG@DMC are a continuous diagonal without slope change with the increase of temperature. As usual, it can be clearly observed a slope change in the ionic conductivity curves of semi-crystal PEO solid polymer electrolyte (Fig. 3b) which is related to PEO crystallization and fusion. When the temperature is around ambient temperature but far below the melting point around 65 °C (much lower when adding LiTFSI), the curves show a near-horizontal line which is due to the existence of crystal region limiting the conduction of Li⁺. Secondly, once the temperature increases near to the melting temperature (from 50 to 70 °C), the slope rapidly changes indicating that ionic conductivity increases rapidly with temperature. Finally, the slope becomes smaller and turns to a near-horizontal morphology again when temperature is much higher than melting point of PEO. These changes strongly indicate that the aggregation state of PEO was changed by the temperature and affected the mode of the transport of Li⁺. In contrast, the ionic conductivity of B-PEG@DMC-15 does not show a violent change against temperature (Fig. 3a), and the Arrhenius plots of B-PEG@DMC-15 are continuous and straight line with no slope change. These indicate that the transport of Li⁺ is no longer restricted by the aggregation state of crystallization but obey the Arrhenius laws shown in Formulas (3 and 4):

$$\sigma = \sigma_0 \exp\left(\frac{-E_a}{RT}\right), \quad (3)$$

$$\lg \sigma = \lg \sigma_0 - \frac{E_a}{2.303RT}, \quad (4)$$

where σ and σ_0 respectively refers to the ionic conductivity and pre-exponential factor, R represents the gas constant, and E_a is the

activation energy reflecting the reorientational dynamics of polymers and could be calculated through Formulas (3 and 4).

On one hand, owing to the PO segment, all the B-PEG@DMC-15 are amorphous with an evenly increasing ionic conductivity curves as the temperature rising. On the other hand, too much PO segment could also limit ionic conductivity. The mass fractions of EO segment in B-PEG@DMC(1100) and B-PEG@DMC(2000) are 10 wt% and 50 wt% in the B-PEG@DMC(2900), meanwhile, it can be clearly observed that the ionic conductivity rises with increase of the weight of EO segment. The B-PEG@DMC(2900)-15 having an O/Li ratio of 15 shows an ionic conductivity of 1.1×10^{-5} S cm⁻¹ at room temperature, whereas the B-PEG@DMC(1100)-15 is 7.6×10^{-6} S/cm and B-PEG@DMC(2000)-15 is 9.3×10^{-6} S/cm (Table S2). Not surprisingly, all the B-PEG@DMC-15 show an ionic conductivity around 10^{-5} S/cm at room temperature with curves highly fitting to Arrhenius formula, which indicates that the restriction of crystal aggregation state has been unblock successfully and Li⁺ conducts mainly through the segmental motion of B-PEG@DMC. Above all, it can be concluded that the aggregation state of B-PEG@DMC is not the main factor to affect the ionic conduction anymore, but the interaction between the ionic mobility and dynamics of chains. Thus, the interaction between Li⁺ and EO segment (PO segment) is discussed in the next paragraph.

In order to investigate how the PO segment influences the ionic conductivity in amorphous state at the molecular level, the molecular dynamics (MD) simulation was performed using Gromacs2018.8 software [36]. The structure of the three polymer models with different weight ratio of EO segment (PEO, B-PEG-10 wt% and B-PEG-50 wt%) are shown in Fig. S2. The molar ratios of the PO segments in the three model molecules are 0, 80% and 44% respectively. The oxygen to lithium ratio is 15:1. The snapshot of simulation box is shown in Fig. 3(d). The simulation results show

that the introduction of PO segment decreases the ionic conductivity over melting point. (1.9×10^{-3} S/cm in PEO, 7.8×10^{-4} S/cm in B-PEG-10 wt% and 2.1×10^{-4} S/cm in B-PEG-50 wt% at 80 °C), which is consistent with experimental results on the trend. The reason could be attributed to the decline of three parameters: u_i (mobility of ion), k (dissociation degree of salt), and c_i^* (molarity of salt) in Formula (5). Firstly, the introduction of PO segments reduces the proportion of dissociated lithium ions (91.1% in PEO, 72.0% in B-PEG-10 wt% and 51.8% in B-PEG-50 wt% as shown in Table S3, due to the weaker coordination ability of PO segment to Li cation than EO segment (in B-PEG-10 wt%, there are 30.6% coordinated oxygen atoms in EO segment and 11.2% coordinated oxygen atoms in PO segment; in B-PEG-50 wt%, there are 39.5% coordinated oxygen atoms in EO segment and 15.2% coordinated oxygen atoms in PO segment). The weaker coordination ability of PO segment may cause by greater dihedral rotation steric hindrance due to the increasing methyl group. This leads to a drop in parameters k . Secondly, the diffusion of oxygen atoms in B-PEG is slower than that in pure PEO, which would slow down the movement of Li ions because of the coupling of Li ion motion and segment motion [43]. In details, the diffusion coefficients of oxygen atoms in PEO, EO segment of B-PEG-10 wt%, PO segment of B-PEG-10 wt%, EO segment of B-PEG-50 wt% and PO segment of B-PEG-50 wt% are 2.27×10^{-7} , 1.75×10^{-7} , 1.14×10^{-7} , 1.58×10^{-7} and 0.81×10^{-7} cm²/s, respectively (shown in Fig. 3c). The lower diffusion coefficient of oxygen atoms in PO segment is also due to the increasing dihedral rotation resistance caused by the methyl side chain. This leads to a drop in parameters

u_i . Thirdly, the increased methyl reduces the molarity of ions when oxygen to lithium ratio is fixed. This leads to a drop in parameters c_i^* .

$$\sigma_i = u_i k c_i^* Z_i F. \quad (5)$$

While the PO segment could effectively unblock the restriction of crystal aggregation state, it could also limit the conduction of Li-ion because of the methyl group. In brief, the B-PEG@DMC(2900) could only conduct Li⁺ in short range. Therefore, in order to further increase the ionic conductivity of SPE, we need to construct a long range Li-ionic conduction pathway. Naturally we compound the B-PEG@DMC(2900) and PEO with low molecular weight ($M_n = 100,000$) to obtain the D-SPE, in which the B-PEG@DMC(2900) could play a role in the transformation of aggregation state from crystal to amorphous and the short range ionic conduction. Meanwhile, low molecular weight PEO could improve the ionic conduction by providing the long range ionic conduction pathway. In this way, we obtained different D-SPE by blending PEO with B-PEG@DMC(2900) with different ratios of LiTFSI (named as PEO- x - y , where x refers to the weight ratio of B-PEG@DMC(2900):PEO; y refers to the ratio of O/Li), aiming to decrease the crystal region (transforming the aggregation state of solid polymer electrolyte) and accelerate the conduction of lithium (introducing a long range ionic conductive pathway) in the D-SPE at the same time. The DSC was used to investigate the thermal properties of D-SPE and pure PEO. In D-SPE, shown in Fig. 4(a), the area of the melting endothermic peaks decreases with the proportion of the B-PEG@DMC(2900) increasing. This demonstrates that crystallinity is decreasing and

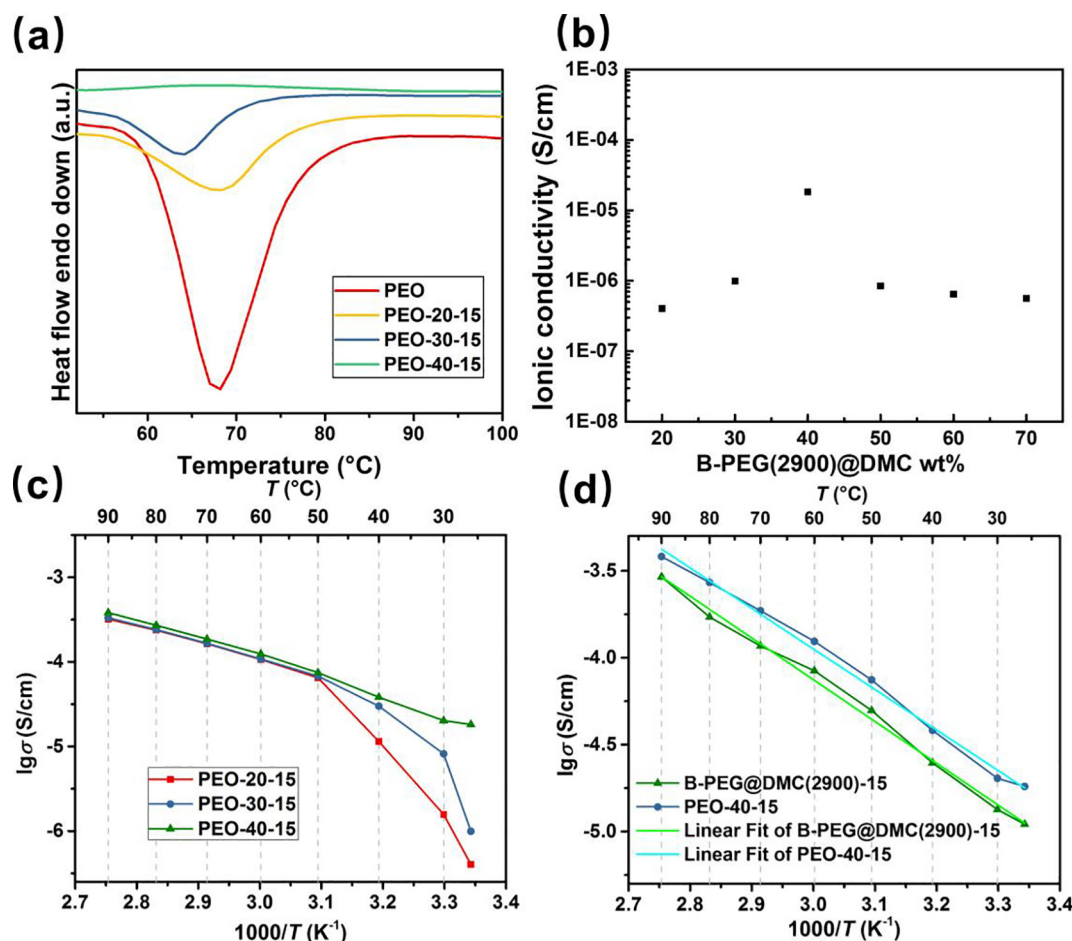


Fig. 4. (a) The DSC of D-SPE with different weight ratios of B-PEG@DMC(2900):PEO. (b) The room temperature ionic conductivity and (c) Arrhenius plots of D-SPE with different weight ratios of B-PEG@DMC(2900):PEO (PEO- x -15). (d) Arrhenius plots of PEO-40-15 and B-PEG@DMC(2900)-15.

then eventually disappears when the B-PEG@DMC(2900) proportion comes to 40%. Nevertheless, the crystallinity change of D-SPE has been calculated according to corresponding endothermic peaks and the crystalline calculation formula (Formula (6)). As expected, the crystallinity of D-SPE (Table S4) clearly decrease with the increasing of B-PEG@DMC(2900) proportion, from 65% (for pure PEO) to 18.9% (for PEO-30–15), and then finally decreased to 0.0% for PEO-40–15.

$$\chi_c = \frac{\Delta H_{\text{exp}}}{\Delta H} \times \frac{1}{w_f} \times 100\%. \quad (6)$$

The ionic conductivity at room temperature (Fig. 4b) and Arrhenius plots (Fig. 4c) of D-SPE with different ratios of B-PEG@DMC(2900):PEO (value of x) are displayed. The curves could be divided into two parts. One is the part before the melting temperature of PEO, it could be clearly observed that the ionic conductivity increases with the increasing value of x due to the crystalline decrease by the adding of B-PEG@DMC(2900), which obviously indicates that the restriction of crystal region is unblock with the addition of B-PEG@DMC(2900) in the D-SPE, this result is strongly consistent with the DSC treatment. The other part is the temperature higher than 50 °C, where the ionic conductivity tends to the same value indicating that D-SPE display a similar conduction behavior as the temperature is higher than melting temperature in which the conduction of Li^+ would not be limited by the crystal region any more but only associated with coupled behavior between oxygen and Li^+ . No surprise, the ionic conductivity of PEO-40–15 has increased due to its amorphous aggregation state, and the ionic conductivity curves of PEO-40–15 (Fig. 4c) eventually shows a monotonic slash demonstrating that the ionic conduction PEO-40–15 is related to Arrhenius equation in all temperature period (from 25 to 90 °C). However, as the addition of B-PEG@DMC2900, too much PO segments would restrict the microscopic conduction of Li^+ as shown in the Fig. 4c, the ionic conductivity of PEO- x - y isn't monotonically increasing with the addition of B-PEG@DMC2900, but reaches the extreme value at PEO-40–15 (2.3×10^{-5} S/cm at room temperature). Unlike B-PEG@DMC, the conduction of Li^+ in D-SPE is improved. Firstly, the B-PEG@DMC(2900) with consecutive PO segment could unblock the restriction of segmental motion caused by crystallinity and also provide a short range ionic conduction pathway. Secondly, PEO rich in EO segment can facilitate the conduction of Li^+ by providing a continuous ionic conduction path. To conclude, the D-SPE could promote the conduction of Li^+ , meanwhile, the ionic conductivity of PEO-40–15 also obey the Arrhenius equation.

As shown in Fig. 4d and Table S5, the linear fitting line and activation energy of B-PEG@DMC(2900) and PEO-40–15 were shown respectively. Obviously, neither B-PEG@DMC(2900) nor PEO-40–15 shows a line highly fitting to Arrhenius law, with the coefficient of determination (R^2) value exceeds 0.99 for all SPE. These indicate that the conduction of Li^+ in B-PEG@DMC and D-SPE is similar with ceramic electrolyte and gel electrolyte which is not limited by aggregation state of polymer but mainly related to segmental motion of the ionic conductive matrix [44]. Both in the cases of B-PEG@DMC and D-SPE, the Arrhenius equation is fitted, indicating that the conduction of Li^+ is only dependent on the segmental motion of the polymer chain [25]. Comparing D-SPE with B-PEG@DMC, in the case of D-SPE, the EO segments and B-PEG@DMC2900 could provide each other oxygen coordination sites which make Li^+ move easier (the glass-transition temperature (T_g) of D-SPE and B-PEG@DMC(2900) were shown in Fig. S12). The decrease of T_g could be contribute to the EO segment of PEO ($M_n = 100,000$) with better segmental motion and coupling motion which has been discussed by the molecular simulation. As expected, the PEO-40–15 shows the best ionic conductivity value of 2.3×10^{-5} S/cm at room temperature (vs. B-PEG@DMC(2900)-15 which shows the ionic conductivity value of 1.1×10^{-5} S/cm at room temperature). Meanwhile, the D-SPE also shows a lower activation energy of 44.63 kJ/mol due to PEO which provides more EO segment and oxygen coordination sites, and also constructs a continuous Li^+ conduction path.

The electrochemical performance of the PEO-40–15 was tested through the assembled battery with lithium iron phosphate (LFP) cathode (Fig. 5) at room temperature. The LFP battery assembled PEO-40–15 as the SPE shows a performance (Fig. 5a) with a stable coulombic efficiency of around 100% and the first charge capacity reaches 148.1 mAh/g which maintains 82% after 70 cycles (as shown in Fig. S9 and S10, the D-SPE shows a stable performance under the rate of 0.2C). It could be observed that capacity descended after 20 cycles with a drop of coulombic efficiency at around 20th cycle, which is attribute to the poor Li^+ conduction channel between SPE and lithium anode caused by the undesirable ionic conductivity of D-SPE at room temperature. Compared to the B-PEG@DMC(2900), D-SPE shows a more stable performance in symmetric cell at 0.1 mA/cm at 25 °C (shown in Fig. S8). At one time, Fig. 5(b) shows the capacity-voltage curves of the 1st, 20th, 50th and 100th, the cell fading with the significant broadening of the potential, due to the polarization problem between electrolyte and lithium anode. The discharge capacity after 100 cycles is still 109.3 mAh/g (73% of 1st cycle).

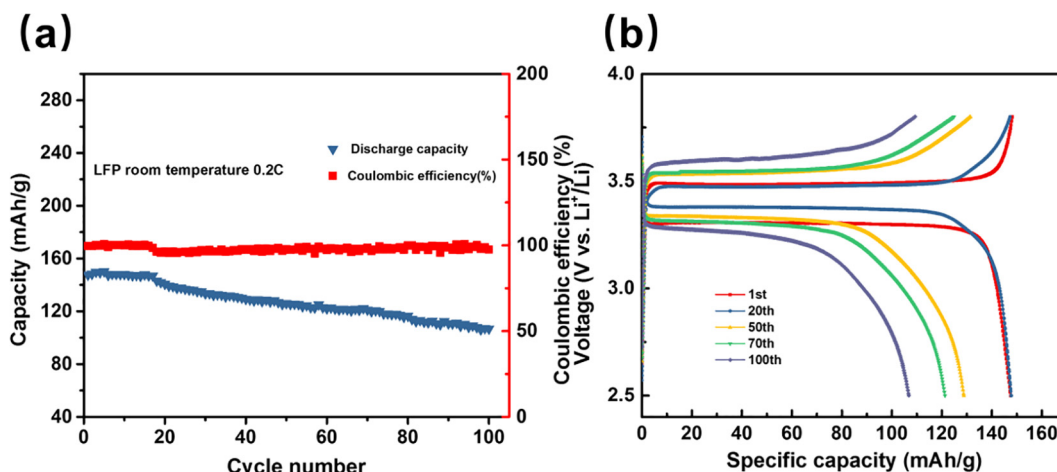


Fig. 5. (a) Cycle performance and (b) charge and discharge curves of the 1st, 20th, 50th, 70th and 100th cycles of the $\text{LiFePO}_4/\text{Li}$ coin cell with optimum D-SPE (PEO-40–15).

Conclusion

In this work, an amorphous SPE with PO block structure (B-PEG@DMC) is synthesized by the transesterification. Firstly, we investigate the thermal property of B-PEG@DMC through DSC that the aggregation state is amorphous, in particular, the weight loss analysis shows that the B-PEG@DMC is solvent-free. Accordingly, the Li^+ could only conduct through the segmental motion of polymer without any effect of solvent. After that, the ionic conductivity curves of B-PEG@DMC(2900) with the addition of LiTFSI are brought out, which shows a fluent slash and fits the Arrhenius formula well. Among them, the B-PEG@DMC(2900)-15 shows the highest ionic conductivity of 1.1×10^{-5} S/cm at room temperature. These verify that the PO segment could effectively unblock the restriction of crystallinity and successfully improve the room temperature ionic conductivity by transforming the aggregation state of polymer. Secondly, we discussed the limitation of PO segment which could only conduct Li^+ in short range as the limit of the steric effect and dihedral rotation resistance caused by the methyl side chain in PO segment. Furthermore, the PEO (long-range ionic conduction) is blended with B-PEG@DMC(2900) (short-range ionic conduction) and obtained a D-SPE to improve the coupled behavior between segments and Li^+ . As expected, the B-PEG@DMC(2900) with PO segments plays role in transformation of aggregation state from crystal to amorphous, meanwhile, the EO segments provide a long-range ionic conduction pathway. The optimum D-SPE is PEO-40-15, with an optimal ratio of B-PEG@DMC(2900) and LiTFSI, showing a well ionic conductivity value of 2.3×10^{-5} S/cm at room temperature. Naturally, it can successfully run in the battery (at room temperature), assembled with LFP cathode and lithium anode for 100 cycles, maintaining the capacity of 109.3 mAh/g (73% compared to 1st cycle).

Declaration of Competing Interest

The authors declare that they have no known competing financial interests or personal relationships that could have appeared to influence the work reported in this paper.

Acknowledgments

The authors gratefully acknowledge financial support from the National Natural Science Foundation of China [22021001, 21875195], the Fundamental Research Funds for the Central Universities [20720190040] and the Key Project of Science and Technology of Xiamen [35022Z0201013]. The authors wish to thank Prof. Weitai Wu of Xiamen University for providing molecular weight measurement and Dr. Xiu Shen of Xiamen University for her kindly supporting. The authors also wish to thanks to the high-Throughput Computational Platform of Chinese Materials Genome Engineering for the high-performance computing resources.

Appendix A. Supplementary data

Supplementary data to this article can be found online at <https://doi.org/10.1016/j.jechem.2021.04.037>.

References

[1] M. Armand, J.M. Tarascon, *Nature* 451 (2008) 652–657.

- [2] D. Bresser, K. Hosoi, D. Howell, H. Li, H. Zeisel, K. Amine, *J. Power Sources* 382 (2018) 176–178.
- [3] B. Dunn, H. Kamath, J.M. Tarascon, *Science* 334 (2011) 928–935.
- [4] Z.Z. Zhang, Y.J. Shao, B. Lottsch, Y.S. Hu, H. Li, J. Janek, L.F. Nazar, C.W. Nan, J. Maier, M. Armand, L.Q. Chen, *Energy, Environ. Sci.* 11 (2018) 1945–1976.
- [5] D. Li, L. Chen, T.S. Wang, L.Z. Fan, *ACS Appl. Mater. Inter.* 10 (2018) 7069–7078.
- [6] R.S. Chen, Q.H. Li, X.Q. Yu, L.Q. Chen, H. Li, *Chem. Rev.* 120 (2020) 6820–6877.
- [7] N. Zhao, W. Khokhar, Z.J. Bi, C. Shi, X.X. Guo, L.Z. Fan, C.W. Nan, *Joule* 3 (2019) 1190–1199.
- [8] D. Zhou, D. Shanmukaraj, A. Tkacheva, M. Armand, G.X. Wang, *Chem.* 5 (2019) 2326–2352.
- [9] Q. Zhao, S. Stalin, C.Z. Zhao, L.A. Archer, *Nat. Rev. Mater.* 5 (2020) 229–252.
- [10] A. Manthiram, X.W. Yu, S.F. Wang, *Nat. Rev. Mater.* 2 (2017) 16103.
- [11] L.S. Li, Y.F. Deng, G.H. Chen, *J. Energy Chem.* 50 (2020) 154–177.
- [12] H. Zhang, C.M. Li, M. Piszcz, E. Coya, T. Rojo, L.M. Rodriguez-Martinez, M. Armand, Z.B. Zhou, *Chem. Soc. Rev.* 46 (2017) 797–815.
- [13] J.M.P.D.E. Fenton, P.V. Wright, *Polymer* 14 (1973) 589.
- [14] S.J. Xu, Z.H. Sun, C.G. Sun, F. Li, K. Chen, Z.H. Zhang, G.J. Hou, H.M. Cheng, F. Li, *Adv. Funct. Mater.* (2020) 2007172.
- [15] K.H. Nie, X.L. Wang, J.L. Qiu, Y. Wang, Q. Yang, J.J. Xu, X.Q. Yu, H. Li, X.J. Huang, L.Q. Chen, *ACS Energy Lett.* 5 (2020) 826–832.
- [16] J. Peng, L.N. Wu, J.X. Lin, C.G. Shi, J.J. Fan, L.B. Chen, P. Dai, L. Huang, J.T. Li, S.G. Sun, *J. Mater. Chem. A* 7 (2019) 19565–19572.
- [17] W. Liu, N. Liu, J. Sun, P.C. Hsu, Y.Z. Li, H.W. Lee, Y. Cui, *Nano Lett.* 15 (2015) 2740–2745.
- [18] H. Gao, Y. Huang, Z. Zhang, J.X. Huang, C. Li, *Electrochim. Acta* 360 (2020) 137014.
- [19] H.Y. Huo, Y. Chen, N. Zhao, X.T. Lin, J. Luo, X.F. Yang, Y.L. Liu, X.X. Guo, X.L. Sun, *Nano Energy* 61 (2019) 119–125.
- [20] J. Jie, Y.L. Liu, L.N. Cong, B.H. Zhang, W. Lu, X.M. Zhang, J. Liu, H.M. Xie, L.Q. Sun, *J. Energy Chem.* 49 (2020) 80–88.
- [21] L.H. Liu, J.S. Mo, J.R. Li, J.X. Liu, H.J. Yan, J. Lyu, B. Jiang, L.H. Chu, M.C. Li, *J. Energy Chem.* 48 (2020) 334–343.
- [22] R. Bouchet, S. Maria, R. Meziane, A. Aboulaich, L. Lienafa, J.P. Bonnet, T.N.T. Phan, D. Bertin, D. Gimes, D. Devaux, R. Denoyel, M. Armand, *Nat. Mater.* 12 (2013) 452–457.
- [23] X. Shen, L. Peng, R. Li, H. Li, X. Wang, B. Huang, D. Wu, P. Zhang, J. Zhao, *Chemelectrochem* 6 (2019) 4483–4490.
- [24] Y.H. Zhang, W. Lu, L.N. Cong, J. Liu, L.Q. Sun, A. Mauger, C.M. Julien, H.M. Xie, J. Liu, *J. Power Sources* 420 (2019) 63–72.
- [25] C. Vancaeyzeele, G.T.M. Nguyen, A.L. Michan, M. Viallon, C.A. Michal, F. Vidal, *Polymer* 142 (2018) 337–347.
- [26] I. Aldalur, H. Zhang, M. Piszcz, U. Oteo, L.M. Rodriguez-Martinez, D. Shanmukaraj, T. Rojo, *J. Power Sources* 347 (2017) 37–46.
- [27] I. Aldalur, M. Martinez-Ibanez, A. Krztoń-Maziopa, M. Piszcz, M. Armand, H. Zhang, *J. Power Sources* 423 (2019) 218–226.
- [28] J. Mindemark, M.J. Lacey, T. Bowden, D. Brandell, *Prog. Polym. Sci.* 81 (2018) 114–143.
- [29] J.H. Zhao, J.J. Zhang, P. Hu, J. Ma, X.G. Wang, L.P. Yue, G.J. Xu, B.S. Qin, Z.H. Liu, X.H. Zhou, G.L. Cui, *Electrochim. Acta* 188 (2016) 23–30.
- [30] J.J. Zhang, J.H. Zhao, L.P. Yue, Q.F. Wang, J.C. Chai, Z.H. Liu, X.H. Zhou, H. Li, Y.G. Guo, G.L. Cui, L.Q. Chen, *Adv. Energy Mater.* 5 (2015) 1501082.
- [31] W.S. He, Z.L. Cui, X.C. Liu, Y.Y. Cui, J.C. Chai, X.H. Zhou, Z.H. Liu, G.L. Cui, *Electrochim. Acta* 225 (2017) 151–159.
- [32] L. Meabe, T.V. Huynh, N. Lago, H. Sardon, C.M. Li, L.A. O'Dell, M. Armand, M. Forsyth, D. Mecerreyes, *Electrochim. Acta* 264 (2018) 367–375.
- [33] I. Aldalur, H. Zhang, M. Piszcz, U. Oteo, L.M. Rodriguez-Martinez, D. Shanmukaraj, T. Rojo, M. Armand, *J. Power Sources* 347 (2017) 37–46.
- [34] I. Aldalur, M. Martinez-Ibanez, M. Piszcz, L.M. Rodriguez-Martinez, H. Zhang, M. Armand, *J. Power Sources* 383 (2018) 144–149.
- [35] I. Aldalur, M. Martinez-Ibanez, A. Krztoń-Maziopa, M. Piszcz, M. Armand, H. Zhang, *J. Power Sources* 423 (2019) 218–226.
- [36] M.J. Abraham, T. Murtola, R. Schulz, S. Páll, J.C. Smith, B. Hess, E. Lindahl, *SoftwareX* 1–2 (2015) 19–25.
- [37] W. Humphrey, A. Dalke, K. Schulten, *J. Mol. Graph.* 14 (1996) 33–38.
- [38] W.L. Jorgensen, D.S. Maxwell, J. Tirado-Rives, *J. Am. Chem. Soc.* 118 (1996) 11225–11236.
- [39] P.M. Anderson, M.R. Wilson, *Mol. Phys.* 103 (2005) 89–97.
- [40] K. Shimizu, D. Almantariotis, M.F.C. Gomes, A.I.A.H. Pádua, J.N.C. Lopes, *J. Phys. Chem. B* 114 (2010) 3592–3600.
- [41] R. Cheerla, M. Krishnan, *Polymer* 155 (2018) 136–145.
- [42] L. Martinez, R. Andrade, E.G. Birgin, J.M. Martinez, *J. Comput. Chem.* 30 (2009) 2157–2164.
- [43] A. Maitra, A. Heuer, *Phys. Rev. Lett.* 98 (2007) 227802.
- [44] E. Quartarone, P. Mustarelli, *Chem. Soc. Rev.* 40 (2011) 2525–2540.